



ISTITUTO NAZIONALE DI RICERCA METROLOGICA Repository Istituzionale

An early Brunhes (<0.78 Ma) age for the Lower Paleolithic tool-bearing Kozarnika cave sediments, Bulgaria

This is the author's submitted version of the contribution published as:

Original

An early Brunhes (0.78 Ma) age for the Lower Paleolithic tool-bearing Kozarnika cave sediments, Bulgaria / Ferrara, Enzo. - In: QUATERNARY SCIENCE REVIEWS. - ISSN 0277-3791. - 178:(2017), pp. 1-13. [10.1016/j.quascirev.2017.10.034]

Availability:

This version is available at: 11696/57207 since: 2018-02-14T15:12:54Z

Publisher:

Elsevier

Published

DOI:10.1016/j.quascirev.2017.10.034

Terms of use:

This article is made available under terms and conditions as specified in the corresponding bibliographic description in the repository

Publisher copyright

(Article begins on next page)

An early Brunhes age for the Lower Paleolithic tool-bearing Kozarnika cave sediments Bulgaria.

Insights on the first peopling of Europe from magnetostratigraphy of the Pleistocene lithic tool-bearing Kozarnika cave sediments, Bulgaria

Giovanni Muttoni¹, Edoardo Monesi¹, Nicholas Sirakov², Jean-Luc Guadelli³, Dennis V. Kent⁴, Giancarlo Scardia⁵, Andrea Zerboni¹, Enzo Ferrara⁶

1 Dipartimento di Scienze della Terra 'Ardito Desio', Università degli Studi di Milano, via Mangiagalli 34, I-20133 Milan, Italy, and ALP - Alpine Paleomagnetic Laboratory, via Luigi Massa, 6, I-12016 Peveragno, Italy.

2 National Institute of Archaeology and Museum of Bulgarian Academy of Sciences, 2, Saborna Street, 1000 Sofia, Bulgaria

3 PACEA/IPGQ-UMR5199 CNRS, Université Bordeaux I, Avenue des facultés, Bâtiment B18, 33405 Talence cedex, France.

4 Earth & Planetary Sciences, Rutgers University, Piscataway, NJ 08854, USA, and Lamont-Doherty Earth Observatory of Columbia University, Palisades, NY 10964, USA.

5 Instituto de Geociências e Ciências Exatas, Universidade Estadual Paulista, Rio Claro, SP 13506-900, Brazil.

6 Istituto Nazionale di Ricerca Metrologica, Nanosciences and Materials Division, INRIM, Torino 10135, Italy

Abstract

We present the magnetostratigraphy of the tool-bearing Kozarnika cave sediments from Bulgaria. Particle size analysis indicates that the silt fraction of the cave infilling is a wind-blown sediment (loess). We found evidence for normal magnetic polarity in the upper part of the section interpreted as a record of the Brunhes Chron, in agreement with small mammal associations from the literature. The Brunhes–Matuyama boundary (0.78 Ma) is placed within Layer 13 Lower, which contains the lowermost levels with Lower Paleolithic

tools. A normal magnetic polarity interval was observed in lowermost Layer 14, dominated by fluvial sands, and was interpreted as a partial record of the Jaramillo subchron (0.99–1.07 Ma). Our results are in substantial agreement with the age of onset of loess deposition in the Danube valley, which occurred shortly before the Brunhes–Matuyama boundary. Moreover, our data indicating Lower Paleolithic tools from levels straddling the Brunhes–Matuyama boundary fits well with a recent hypothesis that hominins first entered Europe across a Danube-Po migration conduit during the late Early Pleistocene.

Introduction

The Kozarnika cave, located in northwestern Bulgaria (**Fig. 1**) yielded a 9 m-thick stratigraphic sequence containing several lithological layers (from Layers 3–5 at the top to Layer 14 at the bottom) (**Fig. 2A**) where various archaeological complexes, spanning from the Neolithic to the Lower Paleolithic have been found (Sirakov et al., 2010 and references therein). The age of the section, based largely on small mammal associations, is however still controversial especially of the inferior layers bearing Lower Paleolithic tools.

Small mammal associations provided a continuous record throughout the section organized, from top to bottom, in (**Fig. 2B**) assemblage A1 (Layers 3a–9b) = “*Arvicola terrestris* Taxon Range zone”, assemblage A2 (Layers 9c–10b) = upper part of “*Lagurus transiens*–*Arvicola cantianus* Assemblage zone”, assemblage B1 (Layer 11a) = “*Mimomys savini*–*Lagurus transiens* Assemblage zone”, and, finally, assemblage B2 (Layers 11b–13) = “*M. savini*–*M. pusillus* Assemblage zone” (Popov and Marinska, 2007). No significant gap seems to be present in this record, which according to standard small mammal bio-magnetochronology should span in relative continuity virtually the entire Brunhes Chron, across the Brunhes–Matuyama boundary (0.78 Ma; ages after Lourens et al., 2004) and into the Jaramillo normal polarity subchron (0.99–1.07 Ma) (Popov and Marinska, 2007). This knowledge is used to erect an expected magnetochronology of the section based on small mammal distribution (**Fig. 2B**).

In contrast, large mammals seem to indicate that the basal Layers 11b–13 should belong to Mammal Neogene/Quaternary (MNQ) zones 19 to 17 (Sirakov et al., 2010; but see also Kahlke, 2011), which, according to a recent radiochronologic ($^{40}\text{Ar}/^{39}\text{Ar}$) reassessment of classic mammalian localities from France, should correspond to a time interval broadly comprised between ~1.2 and ~2.6 Ma (Nomade et al., 2014). In terms of expected magnetochronology, this should straddle the Olduvai normal geomagnetic

polarity subchron (1.78–1.95 Ma) down to the Matuyama–Gauss boundary (2.6 Ma) (**Fig. 2C**).

Magnetostratigraphy coupled with a novel interpretation of the genesis of cave sediments offers the possibility to contribute resolving this conundrum: according to the small mammal age option, we should find predominantly normal magnetic polarity of the Brunhes Chron in the upper half of the cave stratigraphy and evidence for the Brunhes–Matuyama boundary in the lower half of the section, whereas according to the large mammal option, we should find predominantly reverse polarity of the Matuyama Chron possibly straddling the Olduvai normal polarity subchron in the lower half of the section. An actual magnetostratigraphy was previously attempted on the cave deposits but with limited success (Sirakov et al., 2010). Here, we report on the magnetostratigraphy and sedimentology of the Kozarnika deposits and show that neither of these interpretations is strictly correct although our proposed solution is closer to the small mammal age option. These results will be discussed in light of a recent hypothesis that suggests hominins and other mammals first entered Europe across a conjunct Danube-Po migration conduit that opened in the late Early Pleistocene at the onset of the major glaciations in the northern hemisphere.

Cave location and stratigraphy

The Kozarnika cave (Fig. 1) is situated in Bulgaria (district of Belogradchik), in the north-western part of the lower Balkans near the Danubian Plain (Popov, 1933; Sirakov et al., 2010). The cave opens to the south at an altitude of 481 m above sea level on the northern hillside at ca. 85 m above the valley floor of the Skomlia River, a tributary of the Danube River. The Skomlia valley is about 185 m deep and cuts through a Jurassic sequence comprised of Early Jurassic red conglomerates, Middle Jurassic yellow limestones and Late Jurassic grey limestones that host the cave. The stratigraphy of the Pleistocene cave infilling is comprised of the following set of main layers described from top to bottom (**Fig. 2A**; see Sirakov et al., 2010 for details):

- Layers 3a to 4 constitute the uppermost part of the sequence and have not been sampled for magnetostratigraphy. They are altogether 1–1.4 m-thick and composed of calcareous clasts (coming from the cave walls) in a light brown to whitish silty matrix. These layers contain archaeological levels IVb–0I attributed to middle and recent stages of the Kozarnikien, which is a local blade industries containing

backed pieces. Calibrated radiocarbon ages were obtained from uppermost Layers 3a and 3b spanning from 13,160 to 24,460 calendar years BP (Guadelli et al., 2005).

- Layers 5a to 10c are altogether about 1.2-1.5 m-thick. The upper part of this sequence (Layers 5a to 10a), is characterized by yellowish brown silts embedding calcareous clasts and blocks resulting from the fragmentation of the cave walls and roof. Strata underlying Layers 10b and 10c consist of uncompacted dark-brown loamy sand containing gravels and calcareous pebbles showing variable degrees of weathering. In this sequence, Layers 5a-c yielded archaeological levels V–VII attributed to the early stages of the Kozarnikien, and Layer 5b yielded a calibrated radiocarbon age of $31,237 \pm 389$ calendar years BP (Sirakov et al., 2010). Layer 6/7 includes archaeological level VIII, which corresponds to an industry regarded as characteristic of the Middle Paleolithic and the initial Late Paleolithic^[a1], it also yielded uncalibrated, and hence underestimated, radiocarbon ages ranging from 42,700 and 43,600 yr BP (Sirakov et al., 2010). Layers 9a to 10a contain archaeological levels IX–XIII attributed to the Mousterian (Middle Paleolithic) while Layers 10b and 10c contain the lower end of the Mousterian sequence.
- Layers 11a to 13 have a total thickness of about 2.5 m and are composed of rather compact yellowish brown loamy sediments, blotched with dark manganese-bearing nodules and more or less rich in coarse rock blocks and pebbles (limestone blocks, flint pebbles from the cave walls, and more rarely rounded pebbles of quartz) with high degrees of alteration. These layers contain Lower Paleolithic core-and-flake, non-Acheulian industries.
- Layer 14 represents the section base and is characterized by abundant limestone boulders with occasional yellowish brown, laminated sandy matrix in between. Archeological artifacts have not been recovered from this layer.

Sedimentology

Grain size analysis was performed to elucidate the origin of the cave sediments (Gale and Hoare, 1991). A total of 14 samples, ranging in weight from 25 to 40 g, were treated with 10 ml of 30% H₂O₂ in order to remove the organic matter content. This treatment was repeated twice. After drying in an oven at 50°C, samples were gently disaggregated in an agate mortar and sieved at 1000 and 500 µm. Samples were weighted after each step. The fine fraction was then dispersed in 0.05% sodium metaphosphate solution,

disaggregated in an ultrasonic bath for 15 s, and then passed through a Malvern Laser Particle Size Analyser (mod. Mastersizer 2000).

Curves of grain size distribution are reported in **Figure 3** (data in **Supplementary Table 1**), and described hereafter from top to bottom.

- The uppermost Layers 9a-b to 10c display a bimodal distribution of particles: a broad silt mode and high coarse-grained sand ($\geq 1000 \mu\text{m}$) content. The clay content is high in Layers 9a-b to progressively decrease down-section, i.e., the silt mode becomes progressively narrower. This interval is interpreted as a mainly colluvial loess (see also below).
- Curves of Layers from 11a to 13b are very similar and moderately sorted. They present a well-defined silt mode centered at 20–60 μm and high coarse-grained sand ($\geq 1000 \mu\text{m}$) content. A small peak is also present at 120–140 μm and related to fine- to medium-grained sand, while the clay content is always very low. This interval is interpreted as mainly loess deposited into the cave (see also below).
- The lowermost Layer 14 is poorly sorted: it displays a skewed distribution with a long silt tail and a sand mode centered at 100–200 μm as well as high coarse-grained sand ($\geq 1000 \mu\text{m}$) content. This interval consists of mainly colluvial fine-grained sediments (see also below).

Paleomagnetic methods

Results from a previous paleomagnetic sampling were hampered by the unconsolidated nature of the sediments (Sirakov et al., 2010). We avoided this issue by carefully inserting ~5cc plastic cylinders into oriented sediment walls, obtaining a total of 173 specimens for paleomagnetic analyses from Layer 6/7 at the top to Layer 14 at the base (**Fig. 4**). The initial magnetic susceptibility was measured on all weighed samples at room temperature with a KLY-2 Kappabridge. A sub-set of 10 samples was subjected to rock magnetic analyses by means of back-field isothermal remanent magnetization (IRM) acquisition imparted at -2.5 T along the horizontal axis in one direction (-z) and then progressively increasing from +0.025 T up to + 2.5 T in the opposite direction(+z) (Figs. 5A, samples KZ94 and KZ52, 5B, and 5C). Hysteresis analyses were conducted on 6 selected rock chips (mass ~ 40–120 mg) using a Lake Shore 7410 Vibrating Sample Magnetometer (VSM) with maximum applied fields $H_{\text{max}} = \pm 1 \text{ T}$ (Fig.6.A). Hysteresis measurements were repeated after thermal treatment directly applied within the VSM chamber, which is equipped with a thermo-resistance furnace operating in Argon atmosphere used to attain

also thermomagnetic (M vs. T) curves up to 700 °C (applied field $H = 200$ mT). The thermomagnetic curves, showing magnetic moment variations as a function of temperature, offer general information about the magnetic mineralogy, thermal stability, and grain size of the magnetic carriers (Fig. 6.B).

To delineate the magnetostratigraphy, a complete set of samples was subjected to progressive alternating field (AF) demagnetization up to 80 mT. The natural remanent magnetization (NRM) was measured after each demagnetization step with a 2G Enterprises DC-SQUID cryogenic magnetometer located in a shielded room at the Alpine Laboratory of Paleomagnetism of Peveragno and INRIM Turin (Italy). Standard least-square analysis was used to calculate magnetic component directions from vector end-point demagnetization diagrams (Fig.7), and standard Fisher statistical analysis was used to analyze the mean component directions.

Paleomagnetic results

The magnetic susceptibility fluctuates around a mean value of $\sim 20 \cdot 10^{-8} \text{ m}^3/\text{kg}$ throughout most of the section (with one isolated peak value at 6.48 m), while the section base is characterized by higher values of $\sim 40\text{--}60 \cdot 10^{-8} \text{ m}^3/\text{kg}$ (**Fig. 4A**). The intensity of the NRM is comprised between $20 \cdot 10^{-7} \text{ Am}^2/\text{kg}$ and $120 \cdot 10^{-7} \text{ Am}^2/\text{kg}$ (punctuated by an isolated peak value of $242 \cdot 10^{-7} \text{ Am}^2/\text{kg}$ again at 6.48 m) (**Fig. 4B**). IRM acquisition experiments reveal an isotropic behavior of samples. An imparted -2.5 T field along the -z axis produced a parallel IRM, and subsequent fields imparted along the +z axis from +0.025 T up to +2.5 T generated a progressively increasing antiparallel IRM aligned along the +z axis (Fig. 5A, samples KZ94 and KZ52). Only sample KA10 (at 6.48 m) resulted highly anisotropic whereby the IRM generated by the -2.5 T field along the -z axis was found to lie at high angle relative to the -z axis, and subsequent fields along the +z axis produced IRMs again oriented at high angles relative to the +z axis (Fig. 5A, sample KA10). In any case, IRM acquisition curves reveal the presence of a dominant low to moderate coercivity ferromagnetic mineral that tends to saturate in fields of only 0.06 T (60 mT) variably associated with a higher coercivity mineral that shows no tendency to saturate up to 2.5 T fields (**Fig. 5B**). The proportion of soft/hard minerals, isolated following Kruiver et al. (2001), varies throughout the section whereby the hard coercivity fraction is confined to 5–10% of the total IRM from the section's top down to Layer 13b, and then increases to values of up to 20% in Layers 13 Lower and Layer 13/14 (**Fig. 5C**).

Hysteresis loops obtained before thermal treatment show the ubiquitous presence of a soft magnetic phase with very low coercive field ($H_c \sim 10$ mT) associated with a prevalent paramagnetic phase (**Fig. 6A**). After thermal treatment, magnetization and coercive force of the samples increase drastically, resulting in more clearly defined hysteresis loops. As well, magnetic susceptibility values of samples before thermal treatment are about $10\text{--}40 \times 10^{-8}$ m³/kg to increase more than ten times after heating treatment. The heating branches of the thermomagnetic experiments show the presence of a Curie temperature of about 580 °C (**Fig. 6B**) suggestive of magnetite (Dunlop & Özdemir, 1997), in agreement with the results obtained from the IRM experiments. The cooling branches show much higher magnetizations (**Fig. 6B**) probably due to the growth of iron oxides from paramagnetic precursors during heating. No evidence is provided through hysteresis or thermomagnetic experiments of the harder magnetic phase (hematite and/or goethite) revealed by the IRM experiments.

Vector end-point demagnetization diagrams show the presence of soft components of the remanent magnetization termed A that are easily removed between 0 mT and 10–20 mT (**Fig. 7**). These A components are oriented downward (positive inclinations) with scattered, generally northerly declinations (**Figs. 7, 8**). At higher AF demagnetization steps, the NRM becomes harder to release; a characteristic remanent magnetization component, termed C, was isolated in 119 samples, up to a maximum AC field intensity of 80 mT (**Fig. 7**). These C components are either oriented northerly and down, and hence they constitute a sort of a prosecution at higher AF values of the A components, or show a tendency to turn to southerly declinations and upward (negative) inclinations (**Figs. 7, 8**). The bipolar C components, with mean angular deviation (MAD) values of usually lower than 10° (**Fig. 4C**), are grouped around a mean value having declination = 358.3°E and inclination = 62.5° ($n = 119$, $k = 9.8$, $\alpha_{95} = 4.4^\circ$; **Fig. 8**).

Both the A and C components of the NRM are released in AF field intensities that reside well within the IRM acquisition spectrum of the soft coercivity magnetite phase (**Figs. 5,6**). The (subsidiary) hard coercivity phase (hematite and/or goethite), which shows up only in the IRM acquisition experiments and in fields above 100 mT, does not seem to carry any sizable portion of the NRM, which is virtually completely unblocked within fields of 80 mT. This suggests that the C components and the normal and reverse magnetic polarities that they define are carried by the same ferromagnetic (magnetite) phase, irrespective of polarity, which supports the primary nature of these magnetic components.

The declination and inclination values of the C components were used to calculate virtual geomagnetic pole (VGP) latitudes and plotted *versus* stratigraphic depth (**Fig. 4D**). VGP latitudes approaching $+90^\circ$ are interpreted as normal polarity and VGP latitudes approaching -90° as reverse polarity, thus defining a sequence of stratigraphically superposed normal (black) and reverse (white) magnetozones (**Fig. 4E**). The section is characterized by consistent normal magnetic polarity from upper Layers 9a-b at 4.7 m down to 8.28 m within Layer 13 Lower. This relatively thick normal polarity interval is interrupted by anomalous sample KA10 at 6.48 m in the lower part of Layer 11b displaying a southerly-and-up C component direction that is associated with high NRM and susceptibility values (**Fig. 4D, E**); this sample was also highly anisotropic during IRM experiments whereby the induced magnetization lied at high angle relative to the applied fields (**Fig. 5A**). Below meter level 8.28, and still within Layer 13 Lower, as well as in underlying Layer 13/14, reverse polarity C component directions have been observed after removal of a pervasive initial overprint component of normal polarity. At the section bottom, Layer 14 is characterized by C components of normal magnetic polarity (**Fig. 4D, E**).

Discussion

According to grain size distribution curves (**Fig. 3**), the poor sorting of the samples from the uppermost Layers 9a-b and 9c suggests that they consist mainly of colluvial loess (Krumbein and Sloss, 1963; Ricci Lucchi, 1980). The grain size curve of basal Layer 14 also suggests a colluvial origin of the sand-dominated (i.e., non-loess) sediments; moreover, at the macro-scale Layer 14 presents laminated patterns typical of water transport. Samples from intervening Layers 10b to 13b have a characteristic bimodal distribution typical of loess deposited into caves. In fact, the main mode of these curves corresponds to the typical grain size distribution of loess (Pye, 1987, 1995; Coudé-Gaussen, 1990; Assallay et al., 1998), whereas the second peak reflects the presence of sandy to coarser rock fragments from the cryogenic dismantling of the cave walls and roof (**Fig. 3**). A similar bimodal grain size distribution of loess layers has been found in cave entrances and rock shelters at the margin of the Po Plain Loess Basin of northern Italy (Cremaschi, 1987; Castiglioni et al., 1990; Ferraris et al., 1990; Zerboni et al., 2015).

The attribution of most of the analyzed samples to loess trapped at the entrance of the cave fits well with the geographic position of the Kozarnika cave, which is located at the south-western margin of the Bulgarian lower Danube loess belt of eastern Europe

(Buggle et al., 2009, 2013; Fitzsimmons et al., 2012; Markovic et al., 2015; Haase et al., 2007). Loess deposition in the middle and lower Danube valley occurred in the late Early and Middle Pleistocene (Fitzsimmons et al., 2012; Markovic et al., 2015). Considering the several loess sequences and related magnetostratigraphic profiles from Hungary, Serbia, and Romania, we conclude that loess sedimentation generally started in these regions shortly before the Brunhes–Matuyama boundary (Sartori et al., 1999; Jordanova et al., 2008; Fitzsimmons et al., 2012; Markovic et al., 2015; Muttoni et al., 2015a). We consider this the maximum likely age of onset of loess accumulation in the Kozarnika cave, in substantial agreement with our magnetostratigraphic results, as discussed below.

We interpret the thick normal magnetic polarity interval in the upper part of the section as a record of the Brunhes Chron (**Fig. 4D, E**). This interpretation agrees with three independent lines of evidence: (i) the calibrated radiocarbon age of $31,237 \pm 389$ cal yr BP in Layer 6/7 clearly indicates that the section top is latest Pleistocene (= latest Brunhes) in age (Sirakov et al., 2010) (**Fig. 4**); (ii) the small mammal associations indicate that the upper half of the section, from Layers 3a–9b to Layer 11a, should be attributed to the Brunhes Chron (Popov and Marinska, 2007) (**Fig. 2**); (iii) the silt fraction of the cave infilling is a wind-blown sediment (loess); as stated above, the onset of loess deposition in the Danube valley occurred shortly before the Brunhes–Matuyama boundary.

Assuming no substantial gaps throughout the sequence, we place the Brunhes–Matuyama boundary at 8.28 m within Layer 13 Lower (**Fig. 4D, E**). Layer 13 also contains the lowermost levels with Lower Paleolithic tools (Sirakov et al., 2010), which therefore appear to straddle in age the Brunhes–Matuyama boundary (**Fig. 4**). The lower normal magnetic polarity observed in lowermost Layer 14 could be a partial record of the Jaramillo subchron for which, however, we lack a record of its base. The scattered normal polarity directions embedded in the reverse polarity interval within Layer 13 Lower (half bars in **Fig. 4E**) could be manifestations of pre-Brunhes polarity excursions, present-day overprints, or could represent records of the Brunhes Chron in pre-Brunhes sediments due to retarded lock-in of the NRM; it also cannot be excluded that the sedimentologically complex Layer 13 Lower, whose internal stratification/lamination is very hard to trace laterally, contains downward infiltrations (sedimentary dikes/undulated erosional surfaces) of younger (Brunhes) sediments.

Our magnetostratigraphic interpretation does not strictly fit with either of the two working hypotheses shown in **Figure 2**, although it is much closer to the small mammal hypothesis that implies an age of the section base of about 1 Ma (Popov and Marinska,

2007). In particular, the small mammal hypothesis predicts a position for the Brunhes–Matuyama boundary about within Layer 11b instead of Layer 13 Lower where we found it (compare **Fig. 2** with **Fig. 4**). According to previous magnetostratigraphic analyses reported in Sirakov et al. (2010) *"the sedimentation of layers 10a to the middle part of 11b took place in a period of normal magnetic polarity (Brunhes) (...) However the low values of the paleo-latitude in the lower part of layer 11b has been affected by a magnetic transition of inverted polarity (Matuyama) towards normal polarity. Unfortunately, some problems of consolidation of the blocks from the bottom part did not allow continuation of this study"*. Based on this initial report, we paid particular attention to Layer 11b where paleomagnetic sampling resolution was particularly high. We found one sample at 6.48 m in the lower part of Layer 11b displaying reverse polarity; however, the sample magnetic properties were unusual, associated with high NRM values and a highly anisotropic response to IRM experiments. Moreover, however, there is no evidence in this densely sampled interval of a clear and persistent normal-to-reverse polarity transition (**Fig. 4D, E**). Considering our data in conjunction with the virtually continuous small mammal associations as well as the ordered temporal sequence of stone artifacts throughout the section, we see no evidence for substantial stratigraphic gaps and maintain confidence in a Brunhes–Matuyama boundary placed at ~8.28 m or thereabout within Layer 13 Lower (**Fig. 4D, E**).

Conclusions

Our data from Kozarnika, with Lower Paleolithic tools from Layer 11a down to Layer 13 straddling the Brunhes–Matuyama boundary, fits well with a recent hypothesis of first main peopling of Europe centered in a narrow chronological window between the top of the Jaramillo subchron (0.99 Ma) and the Brunhes–Matuyama boundary (0.78 Ma) (Muttoni et al., 2014; 2015a,b). Inspection of **Figure 9** reveals that other sites in Europe with reliable magnetostratigraphic constraints occurring in this time interval are include Gran Dolina in Spain (Pares and Perez-González, 1999; Pares et al., 2013), Sima del Elefante in Spain (Carbonell et al., 2008), Vallparadís in Spain (Martinez et al., 2010), and Monte Poggiolo in northern Italy (Muttoni et al., 2011). Hominin occupation is documented at approximately the same time at the gates of Europe in Israel, such as at Gesher Benot Ya'akov (Goren-Inbar et al., 2000) and Evron (Ron et al., 2003) (**Fig. 9**). Several other sites with evidence of early hominin presence are excluded from this summary either because of poor or poorly documented age constraints (e.g., Soleilhac, Le Vallonnet, Pont-de-Lavaud in

France; Korolevo in Ukraine; Dursunlu in Turkey, and ‘Ubeidiya in Israel), because hominin levels could not be securely traced into the magnetostratigraphic profiles (e.g., Kocabas in Turkey), or because their magnetostratigraphies are incomplete (single polarity only; e.g., Bizat Ruhama in Israel; Pirro Nord in Italy; Happisburgh in the U.K) (see Muttoni et al., 2014; 2015a,b for further details and references).

The oldest peopling of Europe as revealed by the best-dated sites appears to be broadly coeval with the timing of the transition from lower to higher amplitude climate cyclicity that occurred in the late Early Pleistocene between the Jaramillo subchron and the Brunhes–Matuyama boundary (e.g., Head and Gibbard, 2005; Lourens et al., 2004; Lisiecki and Raymo, 2005). Within this climate transition (variably referred in the literature to as late Early Pleistocene Revolution (EPR) or late Early Pleistocene Transition), marine isotope stage (MIS) 22 at ~0.9 Ma represents the first major northern hemisphere continental glaciation of the Pleistocene (Shackleton and Opdyke, 1976; Berger et al., 1993; Shackleton, 1995; Head and Gibbard, 2005). The EPR is believed to have generated for the first time in the Pleistocene vast and exploitable ecosystems for African and Asian mammals especially along a conjunct Danube-Po migration Gateway (Muttoni et al., 2014; 2015a,b) (**Fig. 10**). Enhanced erosion of the Alpine chain by valley glaciers starting with the MIS 22 ice advance and redistribution of these glacial sediments by fluvio-glacial systems from the glaciated mountain areas towards the peripheral plains generated new stable lowland areas along the Danube and Po river valleys. These were colonized by open grassland vegetation and reduced forest cover during the onset of glacial/interglacial transitions starting with MIS 22/MIS 21 (Muttoni et al., 2003; 2010; 2014; 2015a; Scardia et al., 2010; 2012; Monesi et al., 2016). Finally, the EPR coincided also with a profound rejuvenation of the faunas with the substitution of old Villafranchian species by new Galerian elements (Palombo and Mussi, 2006; Palombo, 2014; Muttoni et al., 2014; Monesi et al., 2016).

Putting these and additional factors together, we infer that hominins migrated to Europe from staging areas in the Levant in conjunction with African and Asian mammals as part of a common food web. This faunal assemblage expanded across the newly created grassland-savanna ecosystems of the Danube-Po Gateway, which provided close analogues in the temperate belt of the savanna-type ecosystems to which migrant megaherbivores such as the Asian steppe mammoth (*M. trogontherii*) and the straight-tusked elephant (*E. antiquus*) were already well adapted. Before MIS 22, these lowlands were less suitable for migrating African and Asian megaherbivores because they were

much smaller in extent and were episodically inundated by shallow continental seas and covered by more permanent closed forests (for further details, see Muttoni et al., 2014; 2015a,b; Monesi et al., 2016). This EPR migration scenario is supported by magnetostratigraphic data from Kostolac in Serbia where the first occurrence in Europe of *M. trogontherii* was traced in levels immediately older than the Brunhes–Matuyama boundary (Muttoni et al., 2015a).

Our data from Kozarnika is therefore consistent with the 'follow-the-herd' hypothesis of hominin migration into Europe as part of an ecosystem expanding across a Danube-Po Gateway that was first created in the Pleistocene at ~0.9 Ma during the EPR. Whether hominins occasionally entered Europe already before the Jaramillo (e.g., Carbonell et al., 2008; Toro-Moyano et al., 2013) during times of no particular climatic or ecologic turnover is still a matter of debate (Muttoni et al., 2013; 2015a). In any case, as stressed elsewhere, the regional horizon marking the EPR could represent a prime target for surveys in search of additional sites in the Danube area with mammal immigrants from Asia and Africa (e.g., Kostolac; Muttoni et al., 2015a) possibly including early hominins, like Kozarnika.

Acknowledgements

Aleta Guadelli is warmly thanked for assistance in the field

References

- Assallay, A.M., Rogers, C.D.F., Smalley, I.J., Jefferson, I.F., 1998. Silt: 2–62 μm , 9–4 ϕ . *Earth-Science Reviews* 45, 61–88.
- Berger, W.H., Blickert, T., Schmidt, H., Wefer, G., 1993. Quaternary oxygen isotope record of pelagic foraminifers: Site 806, Ontong Java Plateau. *Proceedings ODP: Scientific Results*, 130, 381–395.
- Buggle, B., Hambach, U., Glaser, B., Gerasimenko, N., Marković, S.B., Glaser, I., Zöller, L., 2009. Magnetic susceptibility stratigraphy and spatial and temporal palaeoclimatic trends in East European loess paleosol sequences. *Quaternary International* 196, 86–106.
- Buggle, B., Hambach, U., Kehl, M., Marković, S.B., Zöller, L., Glaser, B., 2013. The progressive evolution of a continental climate in SE-Central European lowlands during the Middle Pleistocene recorded in loess paleosol sequences. *Geology* 41, 771–774.

- Castiglioni, G.B., Cremaschi, M., Guerreschi, A., Meneghel, M., Sauro, U., Van Vliet, L.B., 1990. The loess deposits in the Lessini plateau. In: Cremaschi, M., (Ed.), The loess in Northern and Central Italy: a loess basin between the Alps and the Mediterranean region. CNR, Milano, 41–59.
- Carbonell, E., Bermudez de Castro, J.M., Pares, J.M., Perez-Gonzalez, A., Cuenca-Bescos, G., Olle, A., Mosquera, M., Huguet, R., van der Made, J., Rosas, A., Sala, R., Vallverdu, J., Garcia, N., Granger, D.E., Martinon-Torres, M., Rodriguez, X., Stock, G.M., Verges, J.M., Allue, E., Burjachs, F., Caceres, I., Canals, A., Benito, A., Diez, C., Lozano, M., Mateos, A., Navazo, M., Rodriguez, J., Rosell, J., Arsuaga, J.L., 2008. The first hominin in Europe. *Nature London* 452, 7186, 465-469.
- Coudé-Gaussen, G., 1990. The loess and loess-like deposits along the sides of the western Mediterranean Sea: genetic and palaeoclimatic significance. *Quaternary International* 5, 1–8.
- Cremaschi, M., 1987. Loess deposits of the plain of the Po and the adjoining Adriatic basin (Northern Italy). In: Pecsli, M., French, H.M., (Eds.), *Loess and Periglacial Phenomena*. Akademiai Kiado, Budapest.
- Dunlop, D.J., Özdemir, Ö., 1997. *Rock Magnetism. Fundamentals and Frontiers*. Cambridge Studies in Magnetism Series. xxi + 573 pp. Cambridge, New York, Port Chester, Melbourne, Sydney: Cambridge University Press.
- Ferraris, M., Sala, B., Scola, V., 1990. The Late Pleistocene fauna with *Pliomys lenki* from the Ghiacciaia cave loess (Northern Italy) *Quaternary International* 5, 71–79.
- Fitzsimmons, K., Marković, S., Hambach, U., 2012. Pleistocene environmental dynamics recorded in the loess of the middle and lower Danube basin. *Quaternary Science Reviews* 41, 104–118.
- Gale, S.J., Hoare, P.G., 1991. *Quaternary sediments*. Belhaven Press, London.
- Goren-Inbar, N., Feibel, C.S., Verosub, K.L., Melamed, Y., Kislev, M.E., Tchernov, E. & Saragusti, I. (2000) - Pleistocene Milestones on the Out-of-Africa Corridor at Gesher Benot Ya'aqov, Israel. *Science*, 289: 944–947.
- Guadelli, J.L., Sirakov, N., Ivanova, S., Sirakova, S., Anastassova, E., Courtaud, P., Dimitrova, I., Djabarska, N., Fernandez, P., Ferrier, C., Fontugne, M., Gambier, D., Guadelli, A., Iordanova, D., Iordanova, N., Kovatcheva, M., Krumov, I., Leblanc, J.C., Mallye, J.B., Marinska, M., Miteva, V., Popov, V., Spassov, R., Taneva, S., Tisterat-Laborde, N., Tsanova, T., (2005). Une séquence du Paléolithique inférieur au Paléolithique récent dans les Balkans: la grotte Kozarnika à Orechets (nord-ouest de

- la Bulgarie). In: Molines, N., Moncel, M.-H., Monnier, J.-L. (eds): Les Premiers Peuplements en Europe, British Archaeological Reports, International Series, 1364: 87 – 103; Oxford (Archaeopress). ISBN: 1841717002
- Dimitrova, I., Djabarska, N., Fernandez, P., Ferrier, C., Fontugne, M., Gambier, D., Guadelli, A., Iordanova, D., Iordanova, N., Kovatcheva, M., Krumov, I., Leblanc, J.C., Mallye, J.B., Marinska, M., Miteva, V., Popov, V., Spassov, R., Taneva, S., Tisterat-Laborde, N., Tsanova
- Haase, D., Fink, J., Haase, G., Ruske, R., Pécsi, M., Richter, H., Altermann, M., Jäger, K.-D., 2007. Loess in Europe – its spatial distribution based on a European loess map, scale 1:2,500,000. *Quaternary Science Reviews* 26, 1301–1312.
- Head, M.J., Gibbard, P.L., 2005. Early–Middle Pleistocene transitions: an overview and recommendation for the defining boundary. In *Early–Middle Pleistocene Transitions: The Land–Ocean Evidence*, Head MJ, Gibbard PL (Eds). Special Publication 247. Geological Society, London, pp. 1–18.
- Jordanova, D., Hus, J., Evlogiev, J. and Geeraerts, R., 2008. Paleomagnetism of the loess/palaeosol sequence in Viatovo (NE Bulgaria) in the Danube basin. *Physics of the Earth and Planetary Interiors*, 167(1), pp.71-83.
- Kahlke, R.-D., García, N., Kostopoulos, D.S., Lacombat, F., Lister, A.M., Mazza, P., Spassov, N., Titov, V.V., 2011. Western Palaeoarctic palaeoenvironmental conditions during the Early and early Middle Pleistocene inferred from large mammal communities, and implications for hominin dispersal in Europe. *Quaternary Science Reviews* 30, 11, 1368-1395.
- Krumbein, W.C., Sloss, L.L., 1963. *Stratigraphy and sedimentation*. Freeman & Co., San Francisco, USA.
- Kruiver, P. P., Dekkers, M. J., & Heslop, D. (2001). Quantification of magnetic coercivity components by the analysis of acquisition curves of isothermal remanent magnetisation. *Earth and Planetary Science Letters*, 189(3), 269-276.
- Lourens, L.J., Hilgen, F.J., Laskar, J., Shackleton, N.J., Wilson, D., 2004. The Neogene Period. In: Gradstein, F.M., Ogg, J.G., Smith, A.G. (Eds), *A Geologic Time Scale 2004*. Cambridge University Press, Cambridge, pp. 409-440.
- Marković, S.B., Hambach, U., Stevens, T., Jovanović, M., O'Hara-Dhand, K., Basarin, B., Lu, H., Smalley, I., Buggle, B., and Zech, M., 2012. Loess in the Vojvodina region (Northern Serbia): an essential link between European and Asian Pleistocene environments. *Netherlands Journal of Geosciences* 91, 173–188.

- Marković, S.B., Stevens, T., Kukla, G.J., Hambach, U., Fitzsimmons, K.E., Gibbard, F., Buggle, B., Zech, M., Guo, Z., Hao, Q., Wu, H., O'Hara Dhand, H., Smalley, I.J., Újvári, G., Sümegi, P., Timar-Gabor, A., Veres, D., Sirocko F., Vasiljević, D.A., Jary, Z., Svensson, A., Jović, V., Lehmkuhl, F., Kovács, J., Svirčev, Z., 2015. Danube loess stratigraphy — Towards a pan-European loess stratigraphic model. *Earth-Science Reviews* 148, 228–258.
- Martínez, K., Garcia, J., Carbonell, E., Agustí, J., Bahain, J.-J., Blain, H.-A., Burjachs, F., Cáceres, I., Duval, M. & Falguères, C. (2010) - A new lower Pleistocene archeological site in Europe (Vallparadís, Barcelona, Spain). *Proceedings of the National Academy of Sciences*, 107: 5762–5767.
- Masini, F., Sala, B., 2007. Large- and small-mammal distribution patterns and chronostratigraphic boundaries from the Late Pliocene to the Middle Pleistocene of the Italian Peninsula. *Quaternary International* 160, 1, 3-56.
- Muttoni, G., Carcano, C., Garzanti, E., Ghielmi, M., Piccin, A., Pini, R., Rogledi, S., Sciunnach, D., 2003. Onset of major Pleistocene Glaciations in the Alps. *Geology* 31, 989-992.
- Muttoni, G., Scardia, G., Kent, D.V., 2010. Human migration into Europe during the Late Early Pleistocene climate transition. *Paleogeography, Paleoclimatology, Paleoecology*, 296, 79-93.
- Muttoni, G., Scardia, G., Kent, D.V., Morsiani, E., Tremolada, F., Cremaschi, M., Peretto, C., 2011. First dated human occupation of Italy at ~0.85 Ma during the Late Early Pleistocene climate transition. *Earth and Planetary Science Letters* 307, 241-252.
- Muttoni, G., Scardia, G., Kent, D.V., 2013. A critique of evidence for human occupation of Europe older than the Jaramillo subchron (~1 Ma): Comment on 'The oldest human fossil in Europe from Orce (Spain)' by Toro-Moyano et al. (2013). *Journal of Human Evolution* 65, 746-749.
- Muttoni, G., Kent, D.V., Scardia, G., Monesi, E., 2014. Migration of hominins with megaherbivores into Europe via the Danube-Po gateway in the late Matuyama climate revolution. *Rivista Italiana di Paleontologia e Stratigrafia* 120, 3, 351-365.
- Muttoni, G., Scardia, G., Dimitrijević, V., Kent, D.V., Monesi, E., Mrdjic, N., Korać, M., 2015a. Age of *Mammthus trogontherii* from Kostolac, Serbia, and the entry of megaherbivores into Europe during Late Matuyama climate revolution. *Quaternary Research* 84, 3, 439-447.

- Muttoni, G., Kent, D. V., Scardia, G., Martin, R. A., 2015b. Bottleneck at Jaramillo for human migration to Iberia and the rest of Europe. *Journal of Human Evolution*, 80, 187-190.
- Nomade, S., Pastre, J.F., Guillou, H., Faure, M., Guérin, C., Delson, E., Debard, E., Voinchet, P. and Messager, E., 2014. 40 Ar/39 Ar constraints on some French landmark Late Pliocene to Early Pleistocene large mammalian paleofaunas: Paleoenvironmental and paleoecological implications. *Quaternary Geochronology*, 21, pp.2-15.
- Palombo, M.R., Mussi, M., 2006. Large mammal guilds at the time of the first human colonization of Europe: the case of the Italian Pleistocene record. *Quaternary International* 149, 94-103.
- Palombo, M.R., 2014. Deconstructing mammal dispersal and faunal dynamics in SW Europe during the Quaternary. *Quaternary Science Review*, 96, 50-71.
- Parés, J. M., Pérez-Gonzalez, A., Rosas, A., Benito, A., Bermudez de Castro, J. M., Carbonell, E. & Huguet, R. (2006) - Matuyama-age lithic tools from the Sima del Elefante site, Atapuerca (northern Spain). *Journal of Human Evolution*, 50: 163–169.
- Parés, J., Arnold, L., Duval, M., Demuro, M., Pérez-González, A., Bermúdez de Castro, J., Carbonell, E. & Arsuaga, J. (2013) - Reassessing the age of Atapuerca-TD6 (Spain): new paleomagnetic results. *Journal of Archaeological Science*, 40: 4586–4595.
- Popov, R., 1933. La grotte Mirizlivka. Contribution à l'étude de la faune diluvienne et de la culture de l'homme quaternaire en Bulgarie, vol. 26. Cahier du musée national d'Archéologie, Sofia, pp. 5–69, (résumé en français).
- Popov, V.V. and Marinska, M., 2007. An almost one million year long (Early to Late Pleistocene) small mammal succession from the archaeological layers of Kozarnika cave in Northern Bulgaria. *COURIER-FORSCHUNGSINSTITUT SENCKENBERG*, 259, p.79.
- Pye, K., 1987. Aeolian dust and dust deposits. Academic, London.
- Pye, K., 1995. The nature, origin and accumulation of loess. *Quaternary Science Reviews* 14, 653–667.
- Ricci Lucchi, F., 1980. Sedimentologia I. Materiali e tessitura dei sediment. CLUEB, Bologna, Italy.
- Ron, H., Porat, N., Ronen, A., Tchernov, E. & Horwitz, L. K. (2003) - Magnetostratigraphy of the Evron Member—implications for the age of the Middle Acheulian site of Evron Quarry. *Journal of Human Evolution*, 44: 633–639.

- Sartori, M., Heller, F., Forster, T., Borkovec, M., Hammann, J., Vincent, E., 1999. Magnetic properties of loess grain size fractions from the section at Paks (Hungary). *Physics of the Earth and Planetary Interiors* 116, 53–64.
- Scardia, G., Muttoni, G., Sciunnach, D., 2006. Subsurface magnetostratigraphy of Pleistocene sediments from the Po Plain (Italy): constraints on rates of sedimentation and rock uplift. *Geological Society of America Bulletin* 118, 11-12, 1299-1312.
- Scardia, G., De Franco, R., Muttoni, G., Rogledi, S., Caielli, G., Carcano, C., Sciunnach, D., Piccin, A., 2012. Stratigraphic evidence of a Middle Pleistocene climate-driven flexural uplift in the Alps. *Tectonics* 31, 6, 1-18.
- Shackleton, N.J., Opdyke, N.D., 1976. Oxygen-isotope and paleomagnetic stratigraphy of Pacific Core V28-239, late Pliocene to latest Pleistocene. *Memoir Geological Society of America* 145, 449-464.
- Shackleton, N.J., 1995. New data on the evolution of Pliocene climate variability. In *Paleoclimate and Evolution, with Emphasis on Human Origins*, Vrba E, Denton GH, Partridge TC, Burckle LH (Eds). Yale University Press, New Haven, pp. 242-248.
- Sirakov, N., Guadelli, J.L., Ivanova, S., Sirakova, S., Boudadi-Maligne, M., Dimitrova, I., Ph, F., Ferrier, C., Guadelli, A., Iordanova, D. and Iordanova, N., 2010. An ancient continuous human presence in the Balkans and the beginnings of human settlement in western Eurasia: A Lower Pleistocene example of the Lower Paleolithic levels in Kozarnika cave (North-western Bulgaria). *Quaternary International*, 223, pp.94-106.
- Toro-Moyano, I., Martinez-Navarro, B., Agustí, J., Souday, C., Bermúdez de Castro, J.M., Martínón-Torres, M., Fajardo, B., Duval, M., Falguères, C., Oms, O., Parés, J.M., Anadón, P., Julia, R., García-Aguilar, J.M., Moigne, A.M., Espigares, M.P., Ros-Montoya, S., Palmqvist, P., 2013. The oldest human fossil in Europe, from Orce (Spain). *Journal of Human Evolution* 65, 1, 1-9.
- Zerboni, A., Trombino, L., Frigerio, C., Livio, F., Berlusconi, A., Michetti, A.M., Rodnight, H., Spötl, C., 2015. The loess-paleosol sequence at Monte Netto: a record of climate change in the Upper Pleistocene of the central Po Plain, northern Italy. *Journal of Soils and Sediments* 15, 1329–1350.

Figure captions

Figure 1. Map of northwestern Bulgaria with location of the Kozarnika cave (43°39' N,

22°44' E).

Figure 2. Lithologic log of the studied Kozarnika cave profile with photographs of the main sampled layers. Panels to the right are the contrasting magnetostratigraphies expected from biozonations of the cave sediments based on small mammals (Popov and Marinska, 2007) or large mammals (Sirakov et al., 2010). Our magnetostratigraphic study aims at resolving this discrepancy while attributing an age to the tool-bearing levels.

Figure 3. Results of laser granulometry of the Kozarnika cave sediments showing a main silt mode attributed to loess in samples from Layers from 11a to 13b while overlying Layers 9a-b to 10c are interpreted as colluvial loess and the lowermost Layer 14 as colluvial non-loessic sediments.

Figure 4. Paleomagnetic data of the Kozarnika cave sediments; from left to the right: lithology log, magnetic susceptibility, natural remanent magnetization (NRM) intensity, mean angular deviation of the characteristic C component, virtual geomagnetic pole (VGP) latitudes and magnetic polarity where black is normal polarity and white is reverse polarity.

Figure 5. (A) Examples of Isothermal remanent magnetization (IRM) acquisition experiments consisting of an initial -2.5 T field imparted along the sample -z axis followed by fields progressively increasing from +0.025 T up to +2.5 T imparted along the +z axis; all samples responded isotropically producing IRMs aligned along the imparted fields except for sample KA10 at 6.48 m that resulted highly anisotropic with IRMs lying at high angles relative to the imparted fields. (B) IRM acquisition curves for representative samples from the Kozarnika cave sediments showing the presence of a dominant low coercitivity magnetic fraction variably associated with a subsidiary hard coercitivity fraction. (C) The soft/hard coercitivity ratios of samples reveal that the hard coercitivity fraction is higher (up to 20% of the total IRM) in Layers 13 Lower and Layer 13/14.

Figure 6. (A) Hysteresis loops before thermal treatment (red curves) and after thermal treatment (black curves) of samples KZ85, KZ68, KZ94, and KF03 showing a paramagnetic phase (positive slope of magnetic moment vs. applied field above 100 mT) coexisting with a soft ferromagnetic phase, which becomes more evident after thermal treatment. (B) Thermomagnetic (heating and cooling) curves for the same samples, showing a Curie point of about 580°C interpreted as due to magnetite. See text for discussion.

Figure 7. Vector end-point demagnetization diagrams of representative samples from the Kozarnika cave sediments. Full symbols are projections on the horizontal plane and open symbols in the vertical plane. Demagnetization temperatures are expressed in °C.

Figure 8. Equal area projection of the A and characteristic C component vectors in *in situ* coordinates from the Kozarnika cave sediments. Full symbols represent down-pointing vectors (normal polarity), open symbols represent up-pointing vectors (reverse polarity).

Figure 9. Our preferred interpretation of evidence for the earliest human occupation of Europe and at the gates of Europe in the Levant with respect to the astrochronological geomagnetic polarity time scale (APTS) (Lourens et al., 2004). Oldest key hominin sites with reliable magnetostratigraphy tend to occur within the reverse polarity interval between the Jaramillo and the Brunhes (0.99 to 0.78 Ma). Europe: Gran Dolina (Pares and Perez-González, 1999; Pares et al., 2013), Sima del Elefante (Carbonell et al., 2008, with cosmogenic burial ages from levels TE7 and TE9 expressed at 2σ level; see discussion in Muttoni et al., 2014; 2015a), Vallparadís (Martinez et al., 2010), Monte Poggiolo (Muttoni et al., 2011), and Kozarnika, Bulgaria (this study). Also shown is the site of Kostolac in Serbia that yielded remains of *M. trogontherii* (but no hominin remains) in pre-Brunhes levels (Muttoni et al., 2015a). Gates of Europe: Gesher Benot Ya'aqov (Goren-Inbar et al., 2000), Evron (Ron et al., 2003). See text for discussion.

Figure 10. Paleogeographic scenario of our revised migrate-with-the-herd hypothesis of earliest expansion of hominins (and large mammals) from the Gates of Europe into Europe across the postulated Danube-Po Gateway during the EPR (dashed lines). Expansion occurred on stable lowlands developed as the Po and Danube deltas prograded over the Adriatic Sea and Black Sea, respectively, since MIS 22 (~0.9 Ma). Coastlines at pre-MIS 22 lowstands and at the last glacial maximum (LGM) are tentatively depicted illustrating the advancement of the Po and Danube deltas. See text for discussion.

Supplementary Table 1. Granulometry data



Figure 1

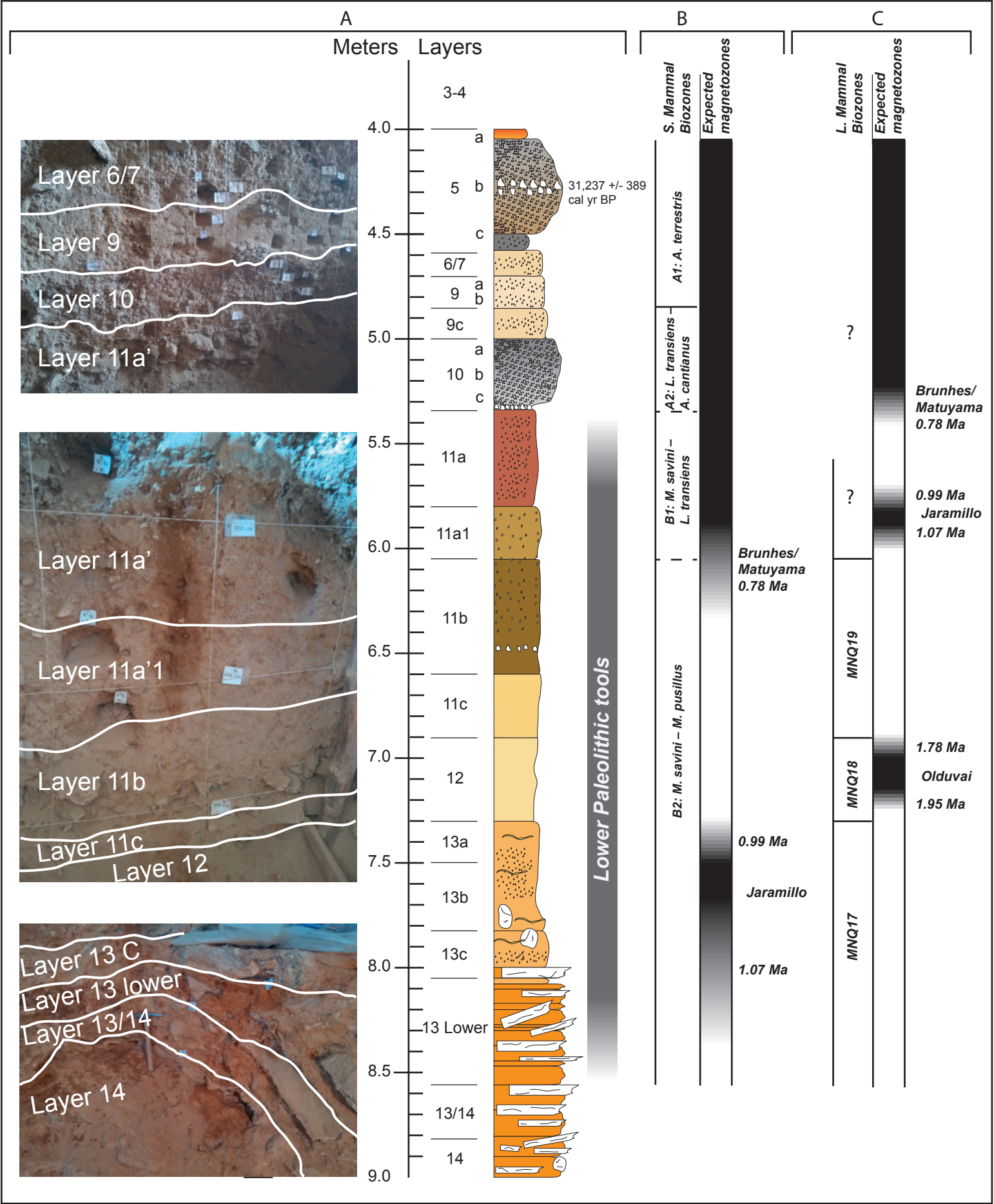


Figure 2

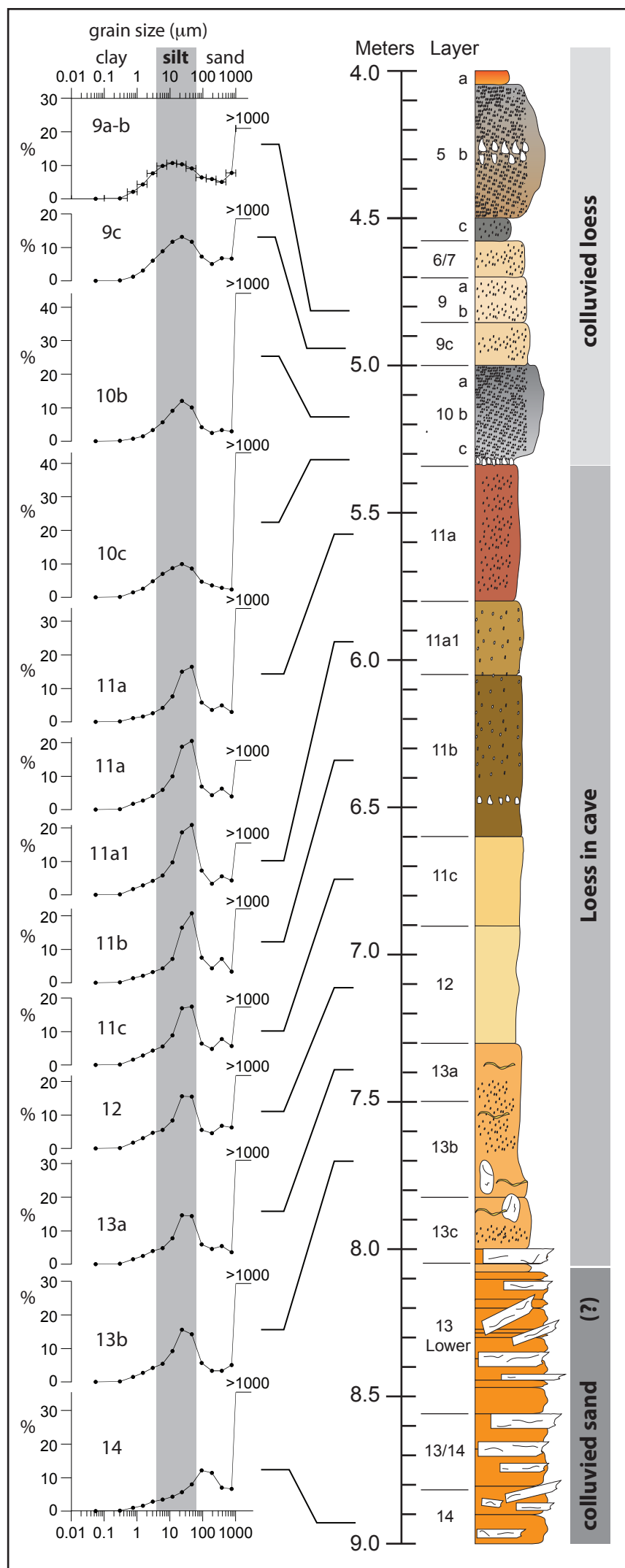


Figure 3

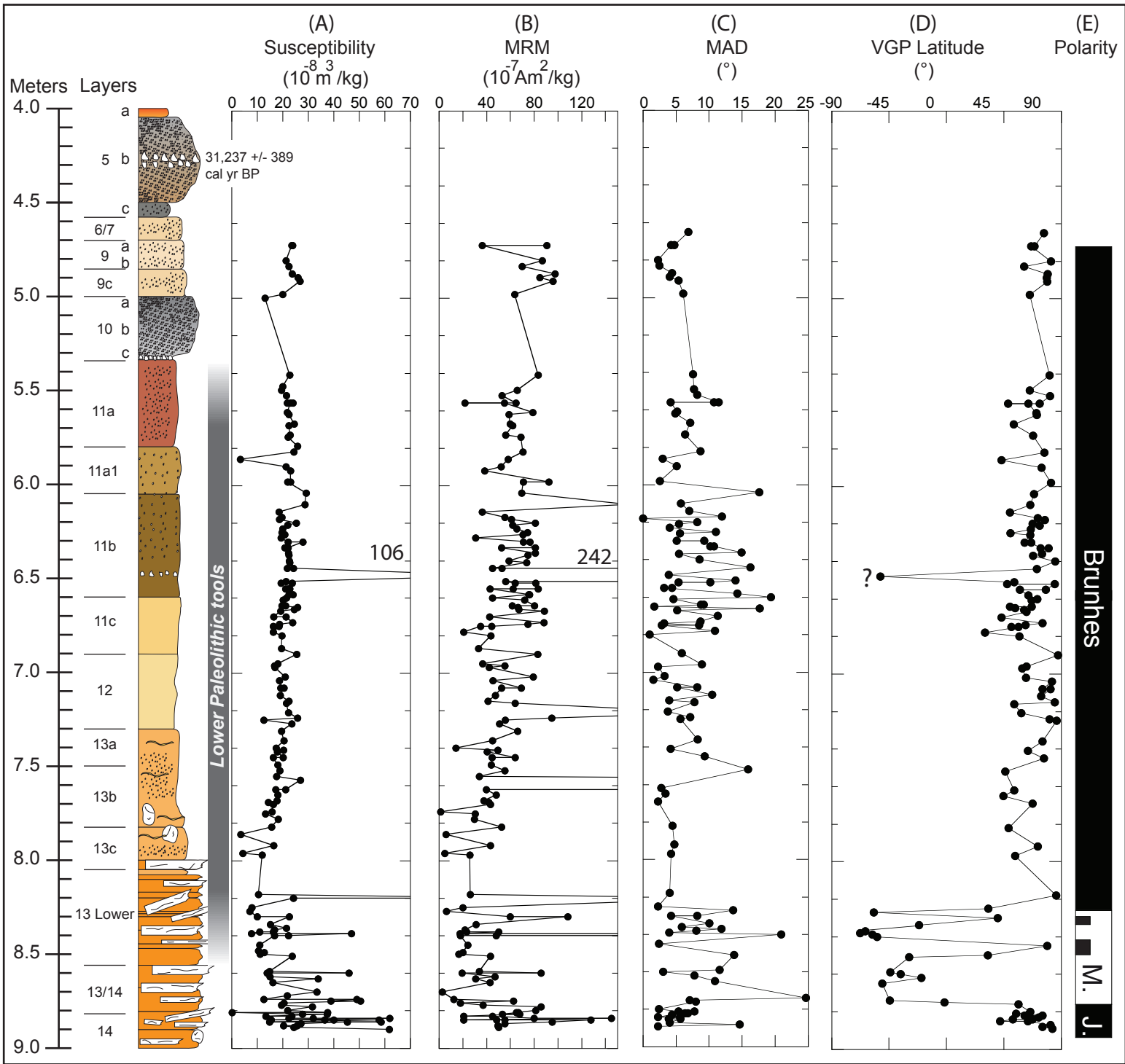


Figure 4

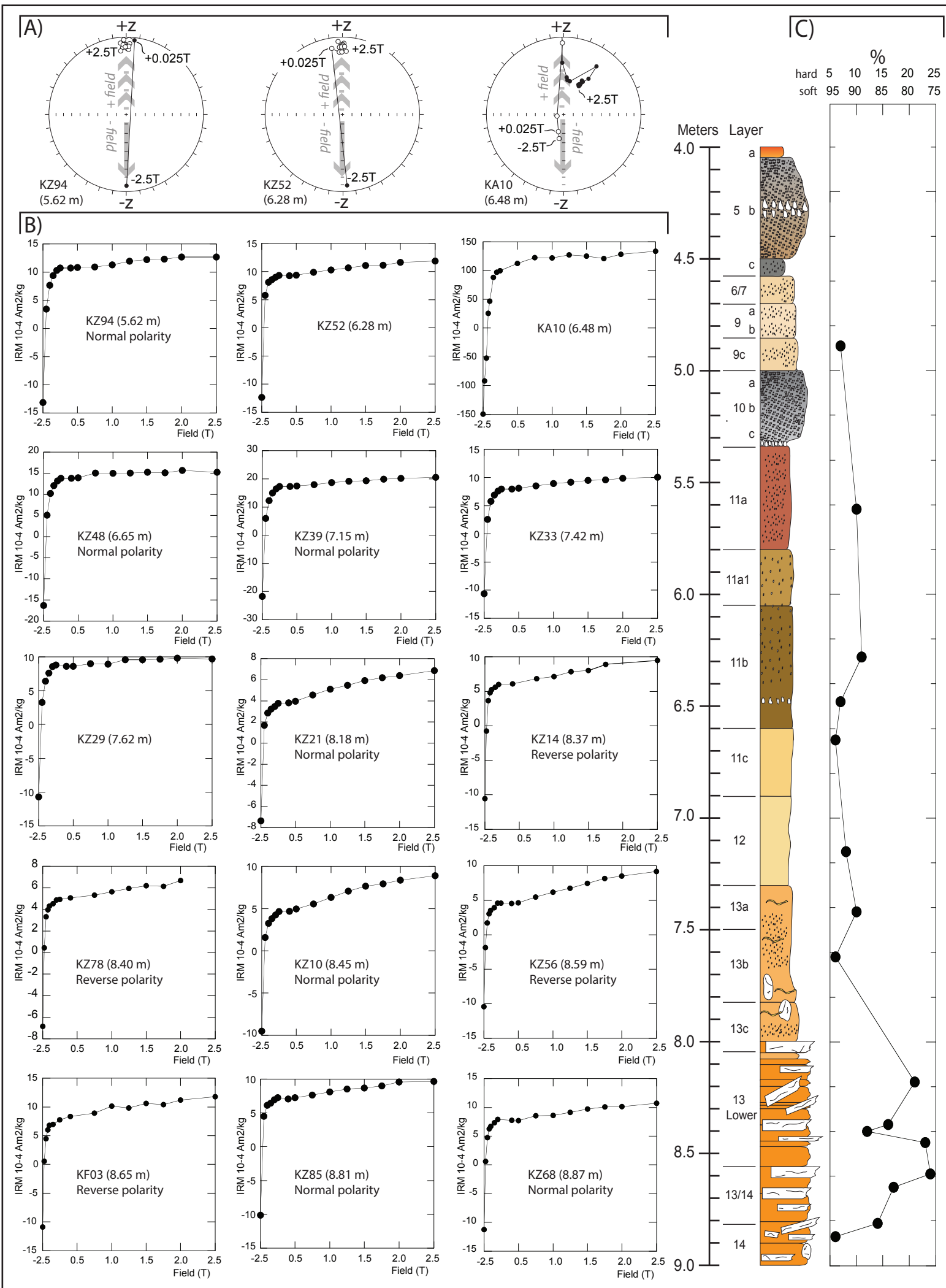


Figure 5

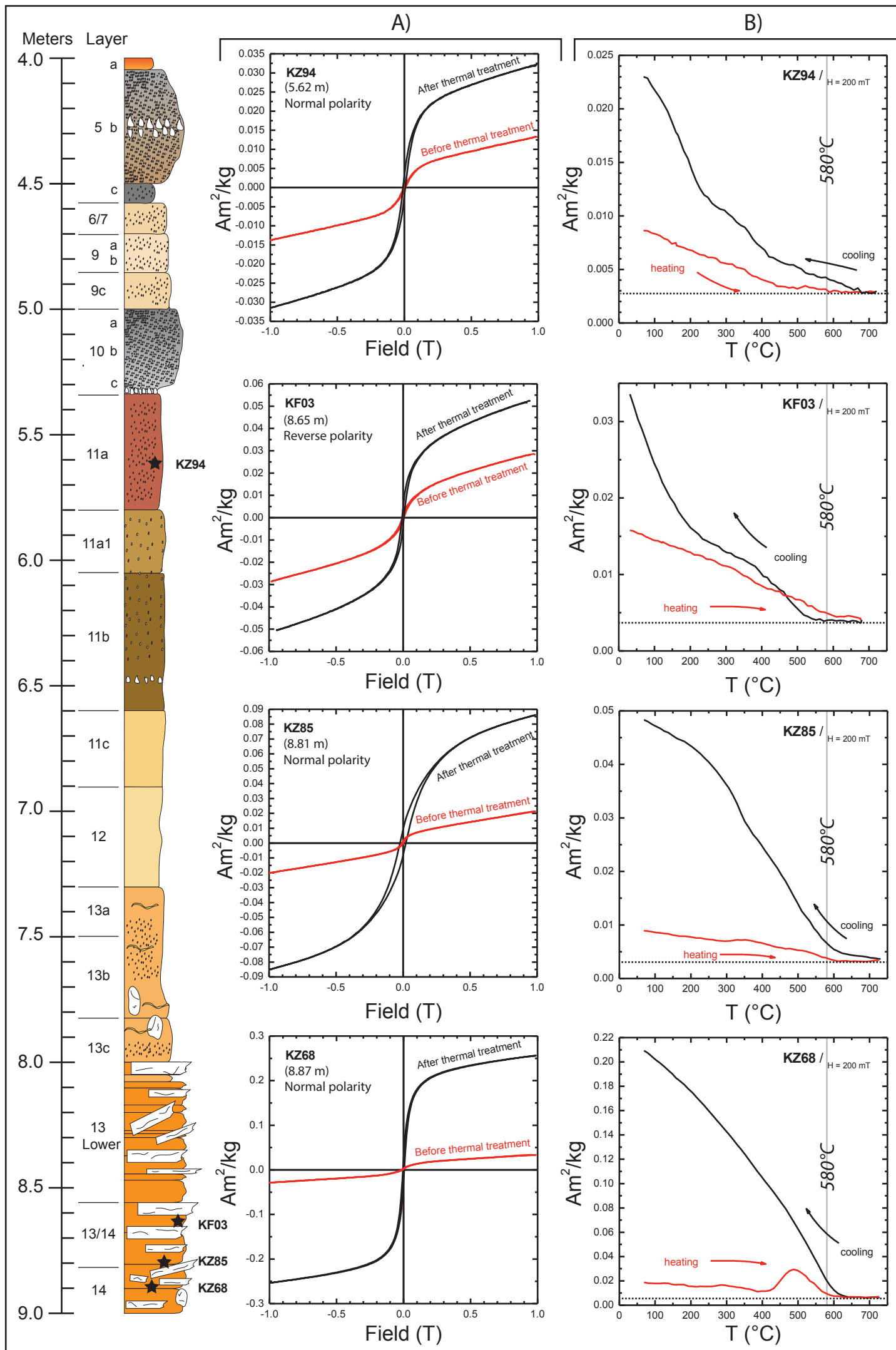


Figure 6

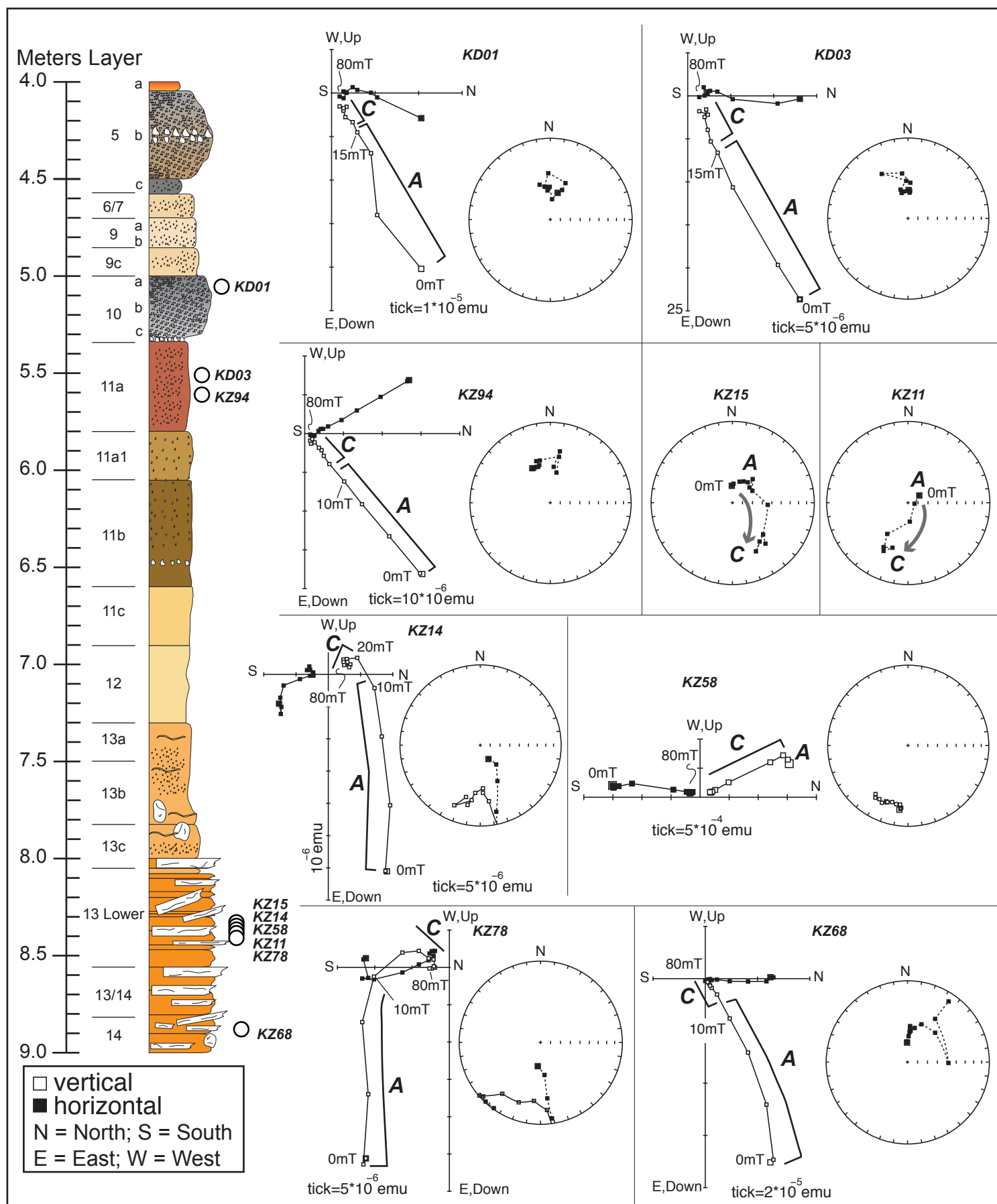


Figure 7

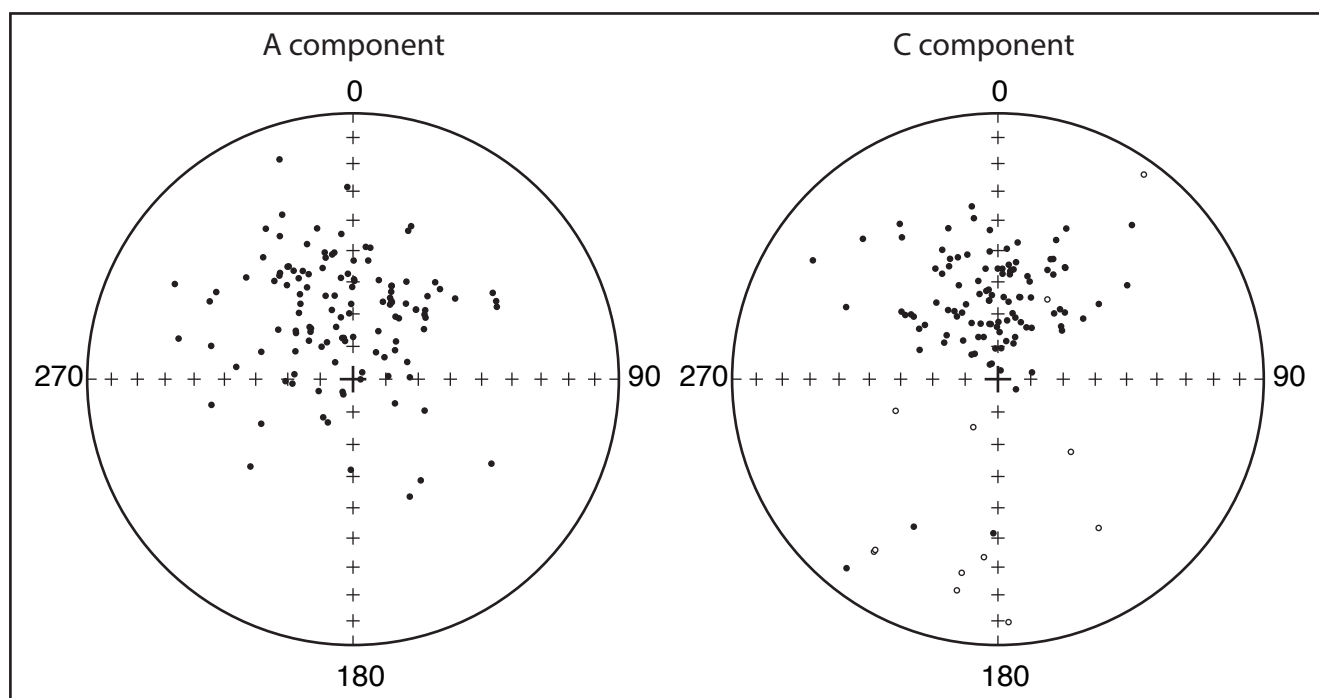


Figure 8

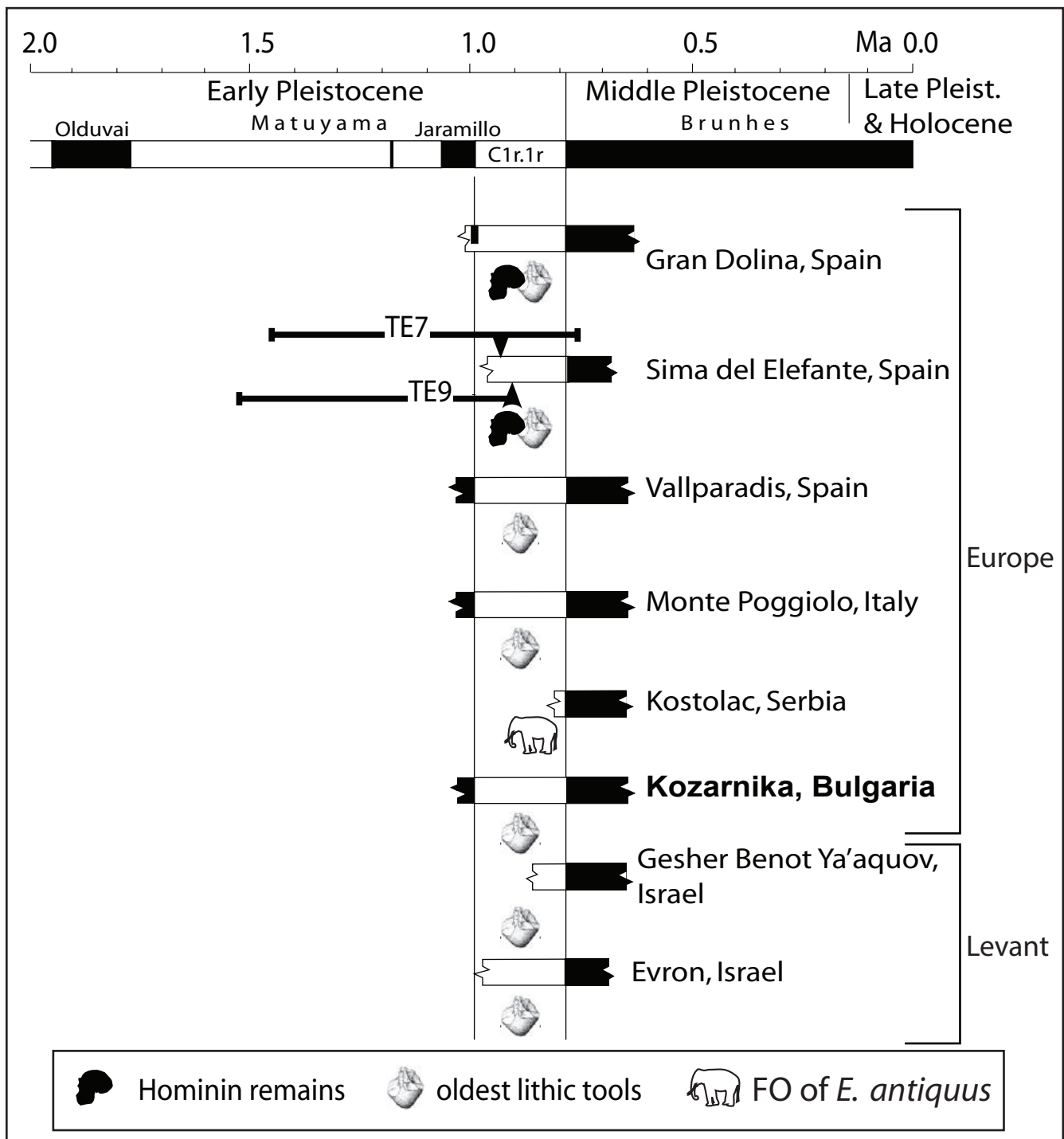


Figure 9

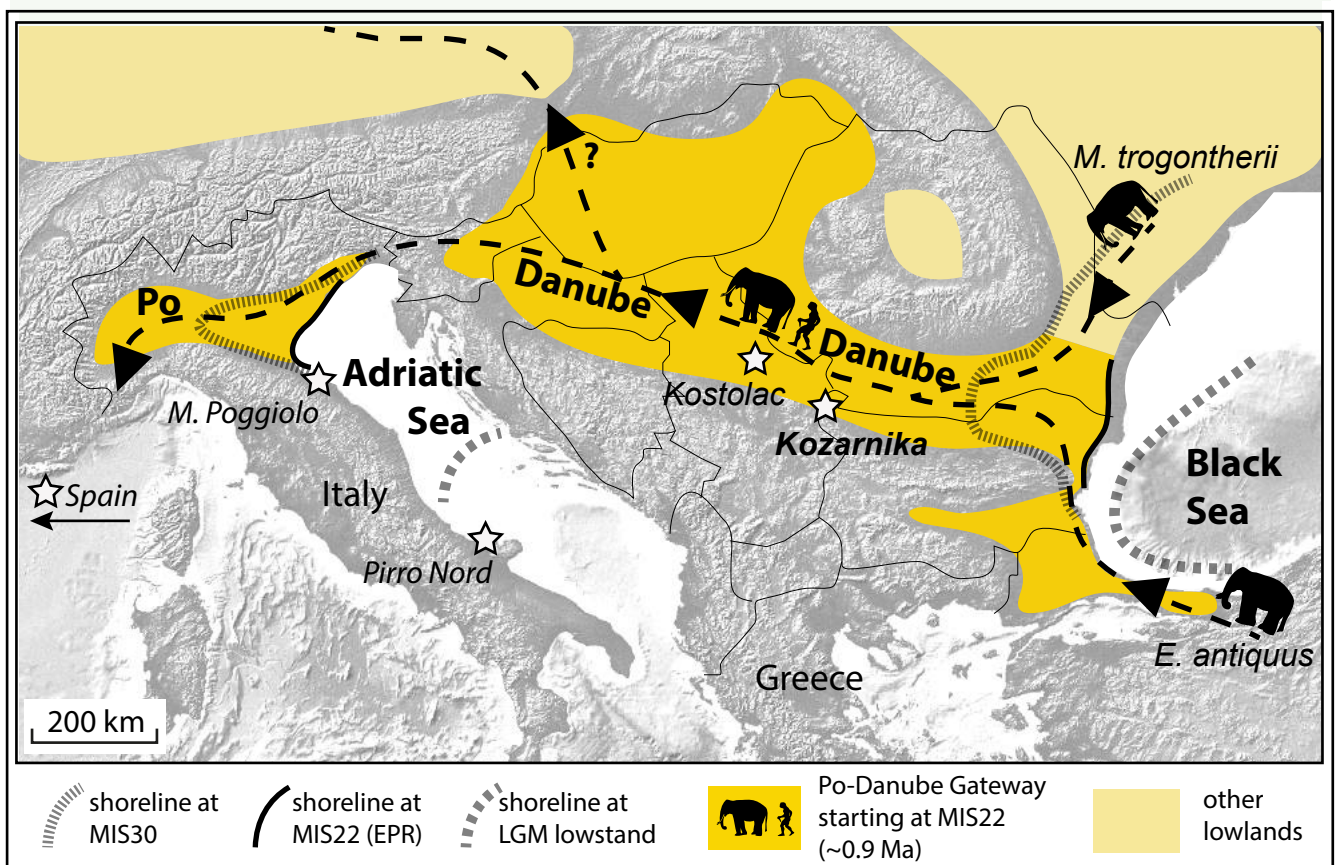


Figure 10